JOURNAL OF MATERIALS SCIENCE 33 (1998) 2203–2214

Microstructural stability, microhardness and oxidation behaviour of *in situ* reinforced Ti–8.5Al–1B–1Si (wt %)

B. G. VELASCO*, P. B. ASWATH
Mechanical and Aerospace Engineering Program and Materials Science and Engineering Program, P.O. Box 19031, University of Texas at Arlington, Arlington, TX 76019, USA

Microstructural stability, microhardness and oxidation behaviour of an *in situ* reinforced Ti–8.5Al–1B–1Si (wt %) alloy was examined in both air and argon environments. When exposed for up to 5760 min at temperatures below the $\alpha/\alpha+\alpha_2$ transius, hardening occurred in both air and argon environments. The increase in hardness in the air heat-treated samples is attributed to a combination of solid-solution strengthening due to the oxygen and the precipitation of the α_2 phase, while the increase in hardness in the argon heat-treated samples is primarily due to the precipitation of the α_2 phase. On the other hand, when heat treated above the $\alpha/\alpha+\alpha_2$ transius, after an initial increase in hardness there is a drop in hardness which is attributed due to elimination of the α_2 phase and a decreased contribution of boron and silicon in the matrix towards the solid-solution strengthening by virtue of coarsening of the $TiSi_2$ and TiB reinforcements. Oxidation of the alloys follows a parabolic oxidation law when oxidized both in an environment of flowing air and static air with the primary oxidation product being TiO_2. The activation energy for oxidation is 200 kJ mol^{-1} in an environment of flowing air and 303 kJ mol^{-1} in static air. The difference in activation energy arises from the difference in the availability of oxygen at the reaction front in the two cases. © *1998 Chapman & Hall*

1. Introduction

The application of conventional titanium alloys (e.g. Ti–6Al–4V, wt %) at high temperature is limited by their metastable microstructure, high oxidation rates and loss of strength. Dispersion strengthening and particle reinforcement of titanium alloys offers the promise of substantial property improvement at elevated temperature. Dispersoids act as barriers to dislocation motion under conditions where thermally activated barriers such as solute atoms, precipitates and grain boundaries are less effective. The application of dispersion strengthening to conventionally processed titanium alloys has only been partially successful, because, addition of large amounts of alloying elements result in a small number of coarse, equilibrium, constituent particles [1–7].

The use of rapid solidification processing (RSP) allows the incorporation of large amounts of additive elements. These added elements can combine with other elements present in the alloy and separate out as dispersoids. Several investigations of particle coarsening in RSP titanium alloys have been conducted [2, 8–11]. Some of the studies involved heat-treated foils [3, 8, 9] and the other studies involved coarsening during extrusion and/or hot isostatic pressing [10, 11]. Studies of coarsening of dispersoids in RSP foils appear to be controlled by volume diffusion [2]. The stability of the post consolidated alloy is of importance for long-term application at elevated temperature.

The reaction of titanium alloys with oxygen at temperatures greater than 550 °C is significant [12]. The resulting damage is not limited to the metal lost to the oxide, but includes the loss of tensile ductility and toughness through incorporation of oxygen into the lattice. It is believed that titanium is embrittled by the presence of as little as 1.2 at % dissolved oxygen. The description of the oxidation process for pure titanium is essentially valid for the alloys of titanium as well; however, the growth rate of the oxide and the oxygen diffusion coefficient in the substrate and in the oxide may be appreciably altered depending on the specific alloy content [12].

In situ reinforced Ti–8.5Al–1B–1Si alloys have exhibited attractive fatigue and fracture behaviour both at room and elevated temperature [13–15]. However, before these materials find engineering application, their stability on long-term exposure to elevated temperature needs to be established. The intent of this work was to evaluate the post-extruded microstructural stability of two kinds of dispersoids: spherical titanium silicides and rod-shaped titanium borides in a Ti–8.5Al–1B–1Si (wt %) alloy. Several heat treatments were made in two different atmospheres,

* *Present address*: University of Lima, Peru.

namely air and argon. In addition, a study was undertaken to characterize the oxidation behaviour of the Ti–8.5Al–1B–1Si (wt %) alloy at several different temperatures and the oxidation behaviour was investigated and reported in this work.

2. Experimental procedure

The material used in this investigation was a super α-based alloy Ti–8.5Al–1B–1Si (wt %; Ti–13.7Al–4B–1.5Si in at %). The actual composition of the alloy is shown in Table I. The material was processed by RSP using a plasma arc-melting/centrifugal atomization (PAMCA) process. The details of the process are provided elsewhere [16]. The powders produced by this technique vary in size from 30–600 μm. The powder was canned in a can made of Ti–6Al–4V and hot pressed. This was then extruded at 955 °C with a reduction ratio of 10:1. In all subsequent studies care was taken to machine the outer can and the diffusion interface.

The extruded product contained spherical titanium silicides and elongated titanium borides. Samples 10 mm × 5 mm × 2.5 mm were cut from the extruded bars and polished with emery paper and weighed. These specimens were annealed at 500, 600, 700, 750, 800, 850 and 900 °C for 120, 1200, 2880, 4320 and 5760 min at each temperature in either an air or argon (99.9% pure) environment, and water quenched. After the heat treatments, the specimens were weighed and sectioned to obtain cross-sectional information of the microstructure. The specimens were mounted in bakelite, polished and etched with Kroll's reagent. Vickers hardness tests (using a Leitz Miniload hardness tester) were made on the mounted samples using a 300 gf test load and the hardness calculated. The average of eight impressions was used.

Particle size and distribution were studied in the scanning electron microscope. The number of particles were determined using an image analyser with Jandil Video Analysis (JAVA™) software and the area of the particles was measured manually using a projection of micrographs and an AUTOCAD™ software.

Oxidation studies involved isothermal tests of specimens with dimensions of 5 mm × 5 mm × 1 mm in the temperature range 600–950 °C for up to 4800 min in a Perkin–Elmer Series 7000 thermal analysis system. An atmosphere of pure air at a flow rate of 50 $cm^3 min^{-1}$ was used. The oxide scale and the base metal were studied using a electron probe microanalyser. In addition, specimens were placed in a closed quartz tube furnace and oxidized for up to 100 h. The oxidation of alloy proceeded by using only the trapped oxygen in the furnace.

TABLE I Composition of the Ti–8.5Al–1B–1Si

Element	Amount (wt %)
Al	8.64
B	1.02
Si	0.99
O	0.11
C	0.13
N	0.022
H	36 (p.p.m.)
Ti	Balance

3. Results and discussion

Ingot metallurgy is not recommended for dispersion, eutectoid or precipitation strengthened titanium alloys because of the coarsening of the dispersoids or precipitates. The problems encountered with *in situ* dispersion strengthening of ingot metallurgy alloys are avoided by RSP. The addition of dispersoid-forming elements to the starting material prior to RSP leads to microstructural refinement and a large number of dispersoids and precipitates. Hence large improvements in both room- and elevated-temperature strength and creep properties can be obtained. Elements added to titanium alloys prior to RSP include, rare-earth elements (e.g. erbium, yttrium, lanthanum) [8, 17], metalloid elements (e.g. boron, carbon, germanium, silicon) [6, 18], and eutectoid formers (e.g. cobalt, nickel, copper) [3, 17]. The rare-earth and metalloids have the potential of forming thermally stable compounds. The rare-earths typically form an immiscible phase, like an oxide, while metalloids prefer to form compounds with titanium. In addition, the rare-earth forming elements scavenge interstitial oxygen, and sulphur, from the titanium matrix depending on the type of rare-earth element. The microstructural stability of the dispersoids is good only as long as the alloys remain in the α phase field, because coarsening is very significant in the β phase field. In addition, particles at grain boundaries tend to coarsen faster [17].

Carbon, boron, silicon and germanium form chemically stable titanium compounds. The addition of silicon to Ti–Al based alloys produces additional solid-solution strengthening in RSP alloys. Attempts to produce titanium alloys with greater than 2.5% Si leads to segregation at grain boundaries. Addition of 0.5–1.5 wt % Si to RSP Ti–Al alloys produces an eutectoid reaction in which $TiSi_2$ intermetallic particles are formed. These particles develop spherical or polyhedral shapes rather than displaying typical eutectoid microstructures. Larger additions of silicon, of the order of 5 wt %, lead to a eutectic decomposition with a fine-scale eutectic microstructure [19]. Boron additions leads to the formation of high aspect ratio filamentary dispersion of TiB particles and a fine grain size [20]. Annealing the RSP ribbons at temperatures between 800 and 900 °C causes coarsening to needle-shaped precipitants and a slight coarsening of the grains. The interstitial elements such as oxygen, nitrogen, carbon and hydrogen have strong affinity to titanium and titanium alloys. Interstitial oxygen occupies the octahedral voids in the h c p lattice resulting in a tetrahedral distortion. In dilute solutions, the oxygen is distributed randomly as single atoms. Depending on the concentration and type of alloy, addition of oxygen produces an increment in the Young's modulus, promotes the formation of α_2 phase (Ti_3Al)

[21] and stabilizes α by raising the $\alpha/(\alpha+\beta)$ and $\alpha/(\alpha+\alpha_2)$ phase boundaries. Oxygen embrittles α-Ti alloys by reducing dislocation glide and changing the slip mode. The majority of the work on the stability and coarsening characteristic of the borides has concentrated on the as-received rapidly solidified ribbons [20], and there is a need for a microstructural stability study on long-term exposure at elevated temperature on the post-consolidated product.

3.1. As-received microstructure

Fig. 1 is a scanning electron micrograph of a polished and etched as-extruded sample. The super α-matrix of this alloy shows small, equiaxed grains. This indicates that dynamic recrystallization occurred during the hot extrusion. During this process, a large number of nuclei of grains form which grow rapidly; however, if they encounter an obstacle, such as a precipitate or a dispersoid, their further growth is impeded as evidenced in the micrograph which shows the presence of spherical particles at the grain boundary. The Ti–Al binary phase diagram, shown in Fig. 2 [22], indicates that under equilibrium conditions, when 8.5 wt % Al is present, small amounts of the ordered α_2 phase should be seen. This is not evident in the micrograph taken on the SEM. In addition, the X-ray diffraction

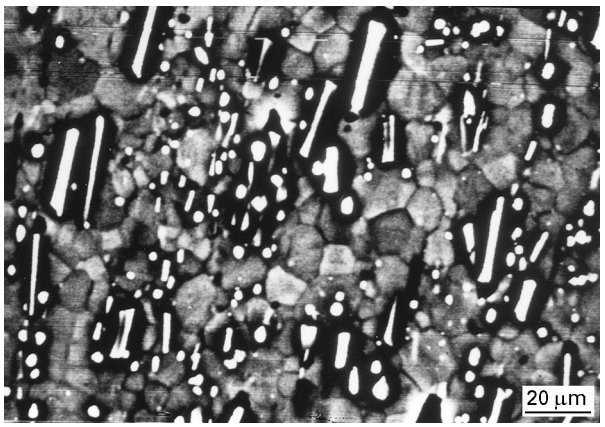

Figure 1 Secondary electron image of the as-received alloy.

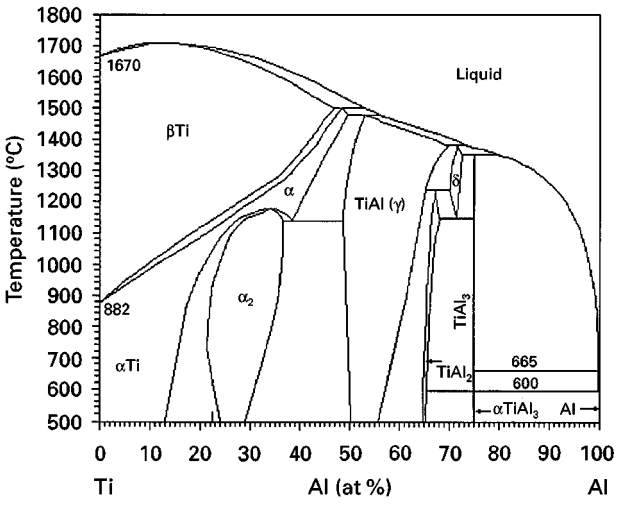

Figure 2 The Ti–Al phase diagram [22].

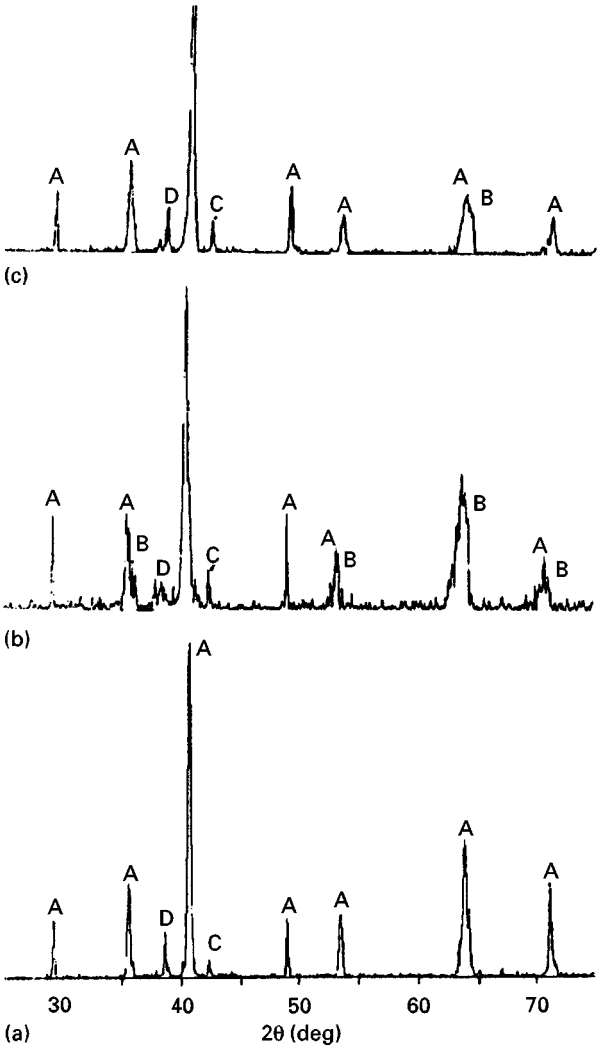

Figure 3 X-ray diffraction peaks of the Ti–8.5Al–1B–1Si, (a) as-extruded material, (b) heat treated in argon at 704 °C for 24 h followed by an air cool, and (c) heat treated in argon at 815 °C for 24 h followed by an air cool. Peaks: A, α phase; B, α_2 phase, C, TiB phase; D, $TiSi_2$ phase.

pattern shown in Fig. 3 also suggests only the presence of an α-phase. The extruded sample was air cooled from 955 °C, which is in the single-phase α region, hence, the α_2 phase may not have precipitated. Results of Gray *et al.* [23] on binary Ti–8.6Al have indicated the presence of small amounts of α_2 in the form of nano-sized dispersoids only visible by transmission electron microscopy. As no transmission electron microscopy was performed, conclusive evidence about the presence or absence of the α_2 phase could not be obtained.

The long rods present in the microstructure are borides of titanium. Observations of the Ti–B binary phase diagram [24] and the X-ray diffraction results in Fig. 3, indicate that these rods are TiB. During conventional casting, the TiB particles typically form as coarse particles from the liquid solution as a eutectic product. Using the RSP route, as in this case, extended solubility of boron is possible. Boron is a strong solid-solution strengthener in alloys formed by RSP. The tetrahedrally coordinated radius of boron is 0.088 nm, lying between the radii of the titanium atom (0.145 nm) and the largest available interstitial position in α-Ti (0.043 nm). The degree of

distortion of the lattice and solution of strengthening per weight per cent are quite high [25]. In the current investigation, RSP ribbons of Ti–8.5Al–1B–1Si were extruded at 955 °C, leading to the formation of rod-shaped TiB particles aligned in the extrusion direction. In addition, spherical-shaped particles identified as compounds of titanium and silicon using electron microprobe analysis were found distributed throughout the matrix with a higher concentration of these particles at the grain boundaries. The Ti–Si binary phase diagram [26], indicates that the possible compound is of the kind Ti_3Si. However, it has been shown by X-ray diffraction in Fig. 3 that due to the sluggishness of the reaction to form Ti_3Si, the product formed is $TiSi_2$. The matrix of this microstructure has a Vickers microhardness of 400 DPH.

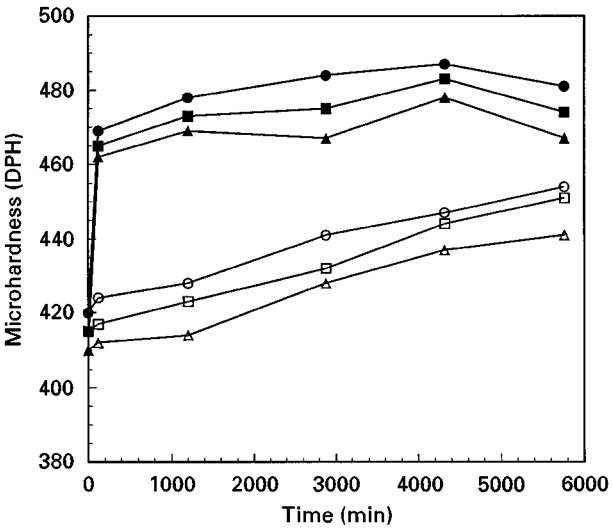

Figure 4 Microhardness of the matrix of the Ti–8.5Al–1B–1Si as a function of heat-treatment time in (■, ●, ▲) air and (□, ○, △) argon at 500 °C: (■, □) mean, (●, ○) maximum, (▲, △) minimum.

3.2. Effect of heat-treatment time on the coarsening behaviour of the dispersoids and microhardness of the matrix

3.2.1. Annealing at temperatures below the $\alpha/\alpha + \alpha_2$ transius temperature

Currently, a quaternary phase diagram that incorporates titanium, aluminium, silicon and boron is unavailable. Boron and silicon are compound formers with titanium and stabilize neither the α phase nor the β phase. It can be assumed, with some approximation, that in small amounts the boron and silicon contents do not have a strong effect on the titanium-rich end of the Ti–Al phase diagram. The aluminum content of 8.5 wt % puts the alloy in the two-phase $\alpha + \alpha_2$ region at $T < 750$ °C. The α_2 phase is an ordered DO_{19} superlattice with a composition Ti_3Al. The presence of the α_2 phase increases high-temperature strength, but significantly reduces low-temperature ductility. The as-extruded samples were annealed at 500, 600 and 700 °C to study the stability and changes in microstructure of the alloy.

At all three temperatures of heat treatments for up to 5760 min in either air or argon, very little change in morphology or grain size was seen. This is contrary to studies of heat treatment of RSP ribbons [6], which contained boron in the solid solution where it was found that the TiB rods that nucleate take up random orientations. In this study the $TiSi_2$ particles are predominantly present at the grain boundaries of the α matrix and hence grain-boundary diffusion appears to aid the coarsening process. Some authors [27, 28] have indicated that α_2 exists as an ellipsoid-shaped particle, changing morphology with the oxygen content. The size scale of the α_2 particles was reported to be of the order of ≈ 0.5 nm [23, 27] which precludes its observation by optical and scanning electron microscopy; however, the X-ray diffraction pattern shown in Fig. 3b indicates the formation of the α_2-phase when the Ti–8.5Al–1B–1Si alloy heat treated at 704 °C in argon for 1440 min followed by air cooling.

Fig. 4 shows the hardness variation as a function of time for samples heat treated in air and argon at 500 °C. The samples heat treated in air show a rapid increase in microhardness to 465 DPH after 120 min which peaks at 4800 min at 482 DPH, followed by a decline. Pure titanium exhibits good affinity to oxygen and α-Ti can absorb as much as 10 wt % oxygen in solid solution [29]. Oxygen stabilizes the α and promotes the formation of the α_2 phase [21]. Because oxygen is a solid solution strengthener, in the presence of α_2, it increases the hardness. In addition, it can be postulated that the α_2 phase precipitates out. On prolonged heat treatment there is coarsening of the $TiSi_2$ and TiB particles. This leads to a depletion of boron and silicon in the matrix leading to a drop in microhardness of the matrix. The samples heat treated in argon show a gradual increase in hardness with time, without exhibiting a peak. The hardness after 5760 min is ≈ 450 DPH. During heat treatment in an argon atmosphere (99.9% pure), the oxygen content is very limited and hence there is a limited increase in hardness due to solid-solution strengthening even after 5760 min heat treatment at 500 °C.

Figs 5 and 6 show the hardness variation as a function of time for samples heat treated in air and argon at 600 and 700 °C, respectively. The microstructure and hardness response is similar to the 500 °C heat treatment. When heat treated in air at 600 °C, the peak hardness is about 465 DPH and occurs after approximately 3000 min heat treatment, and when heat treated at 700 °C the peak hardness is about 470 DPH which was achieved at about 1000 min. At 500 °C, the peak hardness is about 480 DPH and occurs after approximately 4000 min heat treatment. The higher temperature of heat treatment depletes the boron and silicon in the matrix faster, and promotes softening of the matrix. In addition, at higher temperatures, the volume fraction of the α_2 precipitated also decreases.

When heat treated in argon (99.9% pure) at 600 °C there is a gradual increase in hardness which is very similar to the behaviour at 500 °C. At 700 °C, following a gradual increase in hardness up to approximately 4000 min, there is a drop. As the oxygen content in the argon is much smaller than in pure air it leads to the slow increase in hardness. It must be noted that

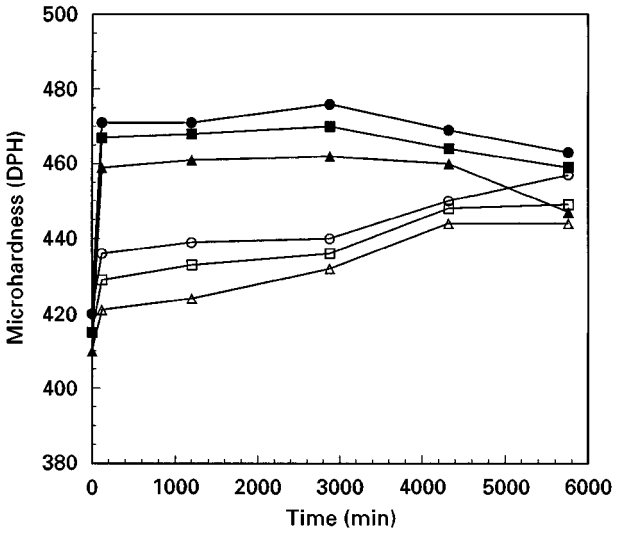

Figure 5 Microhardness of the matrix of the Ti–8.5Al–1B–1Si as a function of heat-treatment in (■, ●, ▲) air and (□, ○, △) argon at 600 °C: (■, □) mean, (●, ○) maximum, (▲, △) minimum.

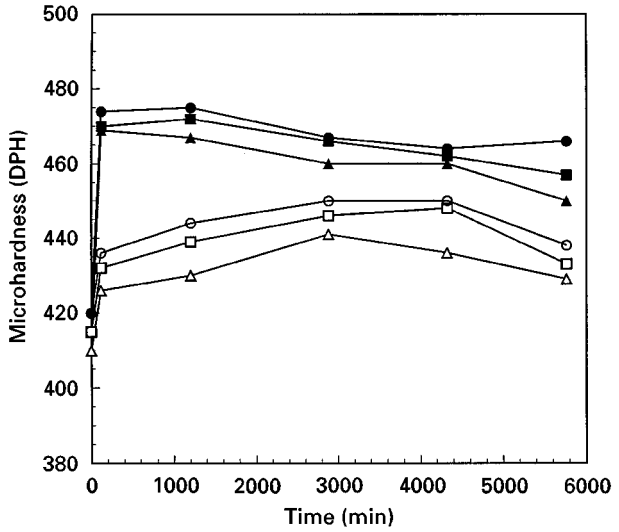

Figure 6 Microhardness of the matrix of the Ti–8.5Al–1B–1Si as a function of heat-treatment in (■, ●, ▲) air and (□, ○, △) argon at 700 °C: (■, □) mean, (●, ○) maximum, (▲, △) minimum.

the maximum hardness achieved in samples heat treated in argon at 700 °C is lower than the minimum hardness seen in the specimen heat treated in air at 700 °C.

3.2.2. Annealing at temperatures above the $\alpha/\alpha + \alpha_2$ transius temperature

Based on the Ti–Al phase diagram, we are in the single-phase α phase field at $T \gtrsim 750$ °C. X-ray diffraction of the extruded Ti–8.5Al–1B–1Si heat treated for 1440 min at 815 °C, followed by an air cool, shown in Fig. 3, indicates the absence of the α_2 phase. The as-extruded samples were annealed at 750, 800, 850 and 900 °C to study the stability and changes in microstructure of the alloy.

3.2.2.1. Annealing at 750 °C in air and argon. The microstructure after heat treatment for 5760 min at 750 °C in air or argon reveals limited changes in morphology. The total number of dispersoids (TiB and $TiSi_2$) initially increases after 20 h annealing followed by a steady decrease for longer times. A summary of the microstructural parameters as a function of heat-treatment time at 750 °C is shown in Figs 7 and 8 for the air and argon heat-treated samples. The significant results in these figures include the following. (i) The number and area fraction of dispersoids shows a maximum at 20 h followed by a steady decline. (ii) In the air heat-treated sample, the number of TiB particles decreased by 20% and area fraction also by 20% on heat treatment for 5760 min, while the number of $TiSi_2$ particles decreased by 50% and the area fraction decreased by 25%. In addition, the mean diameter of the $TiSi_2$ particle increased by 30%. (iii) Heat treatments in air and argon show similar trends. A plot of $F = \bar{d}^4 - \bar{d}_0^4$ versus time (where $\bar{d}$ is the mean diameter of a $TiSi_2$ particle at time $t = t$ and $\bar{d}_0$ is the mean diameter of a $TiSi_2$ particle at time $t = 0$ when the sample is heat treated at 750 °C) yields a straight line for both the air and argon heat-treated samples. The

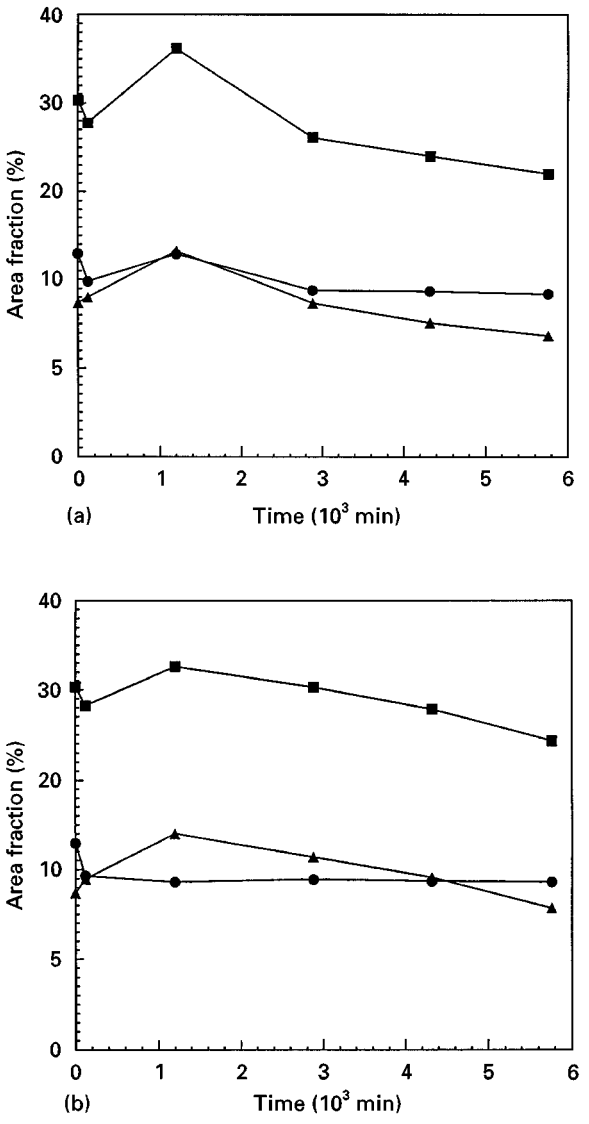

Figure 7 Area fraction of dispersoids as a function of heat-treatment time in (a) air and (b) argon at 750 °C. (■) Total dispersoids, (●) TiB particles, (▲) silicide particles.

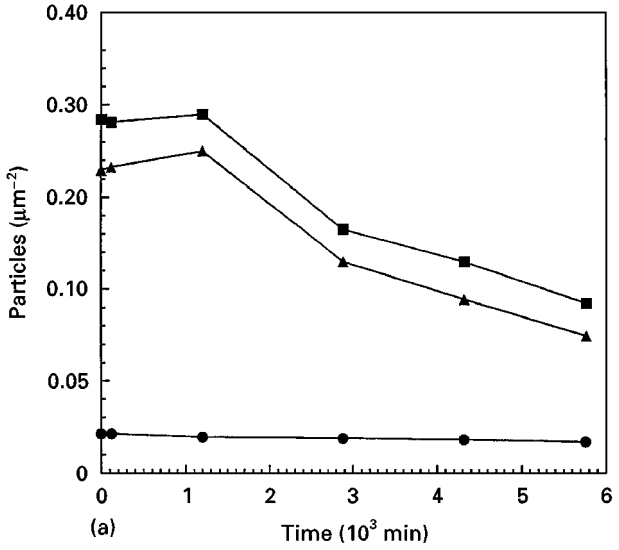

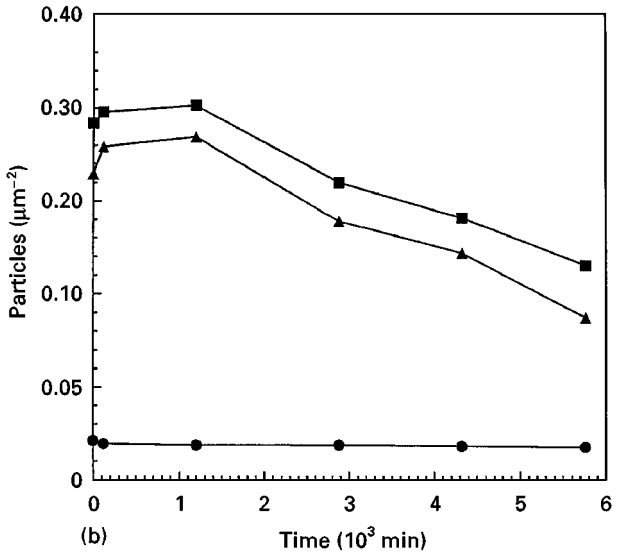

Figure 8 Number of particles per square micrometre as a function of heat-treatment time in (a) air and (b) argon at 750 °C. (■) Dispersoids, (●) TiB rods, (▲) silicide particles.

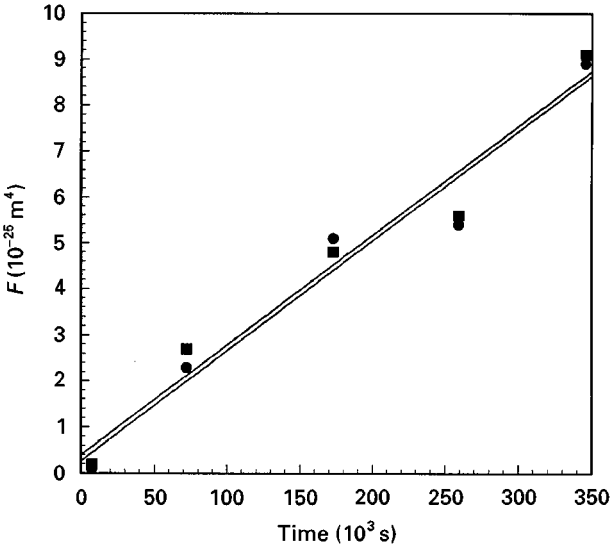

Figure 9 Plot of F of the $TiSi_2$ particles as a function heat-treatment time at 750 °C in air and argon, where $F = d^4 - \bar{d}_0^4$, and $d_0 = TiSi_2$ particle size at $t = 0$ and $d = TiSi_2$ particle size at time $t = t$. (■) Air and (●) argan.

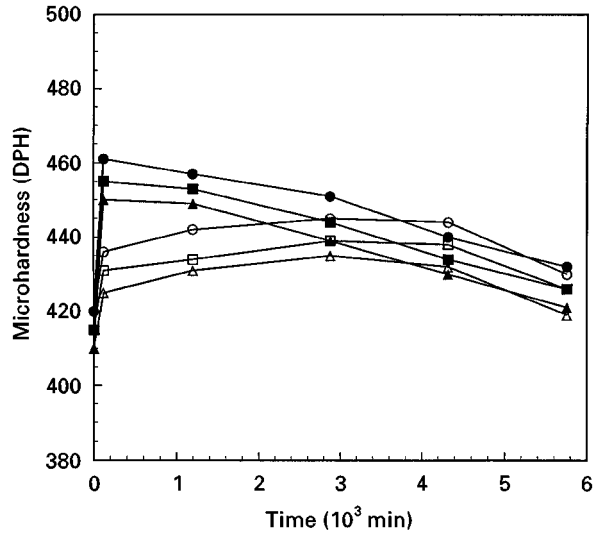

Figure 10 Microhardness of the matrix of the Ti–8.5Al–1B–1Si as a function of heat-treatment in (■, ●, ▲) air and (□, ○, △) argon at 800 °C: (■, □) mean, (●, ○) maximum, (▲, △) minimum.

coarsening behaviour exhibits a relationship of the kind $F = \bar{d}^4 - \bar{d}_0^4$. Fig. 9 shows a plot of F versus time for air and argon, respectively. The slope of the plots yields k, the rate constant for coarsening ($F = kt$). The $TiSi_2$ particles are predominantly present at the grain boundaries while the TiB particles are scattered throughout the matrix. Coarsening of $TiSi_2$ particles is promoted by grain-boundary diffusion. Bhattacharya and Russell [30] have shown that k can be expressed in the form

$$k = \frac{(D_b C_b)\delta\gamma V_m^2}{RT} \quad (1)$$

where V_m is the molar volume of a particle, γ the particle/matrix interfacial energy, δ the grain-boundary thickness, D_b the grain-boundary diffusion coefficient of the active species, and C_b the component solubility in the grain boundary.

There is little difference in the k values for air and argon heat-treated samples ($k = 2.38 \times 10^{-30}\ m^4\ s^{-1}$ in air and in argon at 750 °C) and hence it can be inferred that oxygen does not play a significant role in the coarsening behaviour of the $TiSi_2$ particles. In addition, it should be noted that the coarsening rate of these particles is very slow at 750 °C. It is known that silicon diffuses faster in β-Ti (b c c) compared to α-Ti (h c p) [31]. In this study it was found that the coarsening rate increased rapidly as the temperature was raised into the two-phase α + β region.

3.2.2.2. Annealing at 800, 850 and 900 °C. Figs 10, 11 and 12 show the hardness variation as a function of time for samples heat-treated in air and argon at 800, 850 and 900 °C. The microstructure after 5760 min heat treatment is very similar to that formed after the treatment at 500 °C for 5760 min. However, the microhardness of the matrix shows some distinct

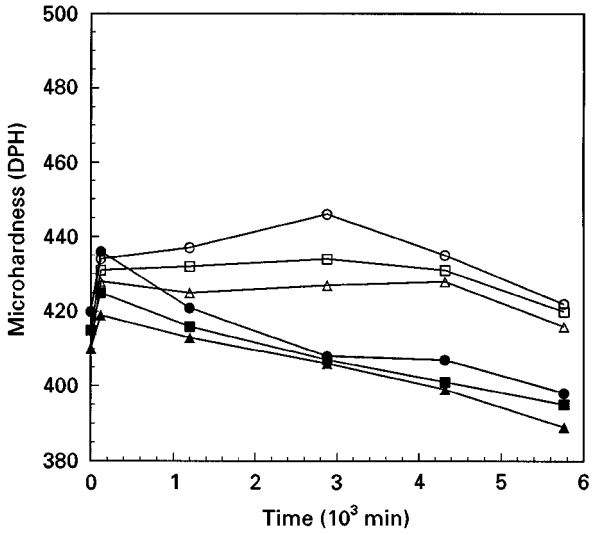

Figure 11 Microhardness of the matrix of the Ti–8.5Al–1B–1Si as a function of heat-treatment in (■, ●, ▲) air and (□, ○, △) argon at 850 °C: (■, □) mean, (●, ○) maximum, (▲, △) minimum.

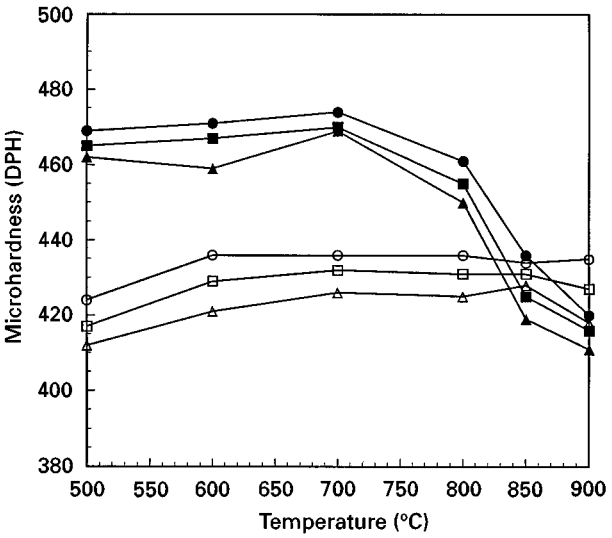

Figure 13 Microhardness of the matrix of the Ti–8.5Al–1B–1Si as a function of heat-treatment temperature for samples heat treated in (■, ●, ▲) air and (□, ○, △) argon for 120 min: (■, □) mean, (●, ○) maximum, (▲, △) minimum.

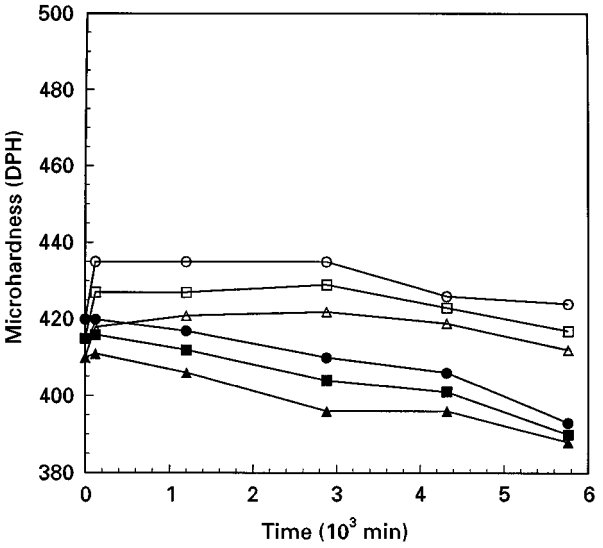

Figure 12 Microhardness of the matrix of the Ti–8.5Al–1B–1Si as a function of heat-treatment time in (■, ●, ▲) air and (□, ○, △) argon at 900 °C: (■, □) mean, (●, ○) maximum, (▲, △) minimum.

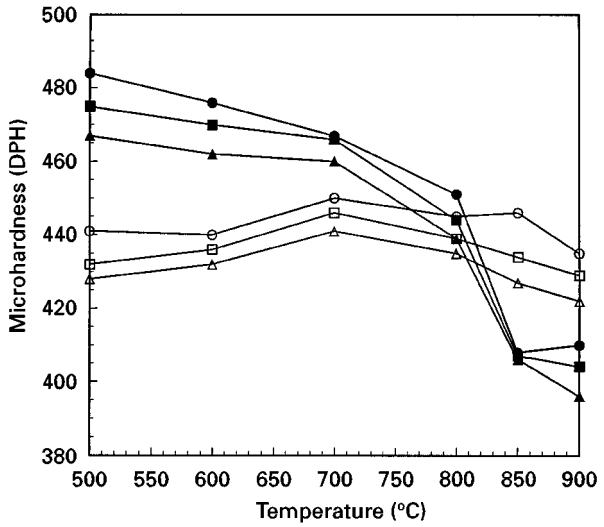

Figure 14 Microhardness of the matrix of the Ti–8.5Al–1B–1Si as a function of heat-treatment temperature for samples heat treated in (■, ●, ▲) air and (□, ○, △) argon for 2880 min: (■, □) mean, (●, ○) maximum, (▲, △) minimum.

dissimilarities. At 800 °C, the samples heat treated in air show an initial increase to 450 DPH after 100 min, after which there is a monotonic decrease. When heat treated in argon, the peak in hardness occurs at 4000 min after which there is a drop. The hardness after 5760 min is identical in both air and argon environments. At 850 and 900 °C, the samples heat treated in air show a rapid decrease in hardness to a value that is below the hardness of the non-heat-treated alloy. However, the samples that were heat treated in argon did not show much of a variation in hardness even after 5760 min heat treatment.

3.3. Effect of temperature on the microhardness of the matrix

Figs 13, 14 and 15 represents the variation of microhardness with temperature of heat treatment for samples heat treated for 120, 2880 and 5760 min, respectively. In samples heat treated in air for 120 min, the microhardness is insensitive to annealing temperature up to 700 °C, after which there is a rapid decrease in hardness. The argon heat-treated samples shows an increase in hardness which levels off at temperatures above 700 °C. Samples heat treated for 2880 min in air exhibit a gradual decrease in hardness with an increase in temperature in the range 500–700 °C. At $T > 700$ °C there is a rapid decrease in hardness. In the samples heat treated in argon, the hardness is almost steady in the 500–800 °C range at ≈ 430 DPH followed by a small drop at $T > 800$ °C. In samples heat treated for 5760 min in air the microhardness drops from a peak value of ≈ 475 DPH at 500 °C to ≈ 390 DPH at 900 °C while the argon heat-treated sample experiences a constant hardness of ≈ 450 DPH in the temperature range 500–600 °C

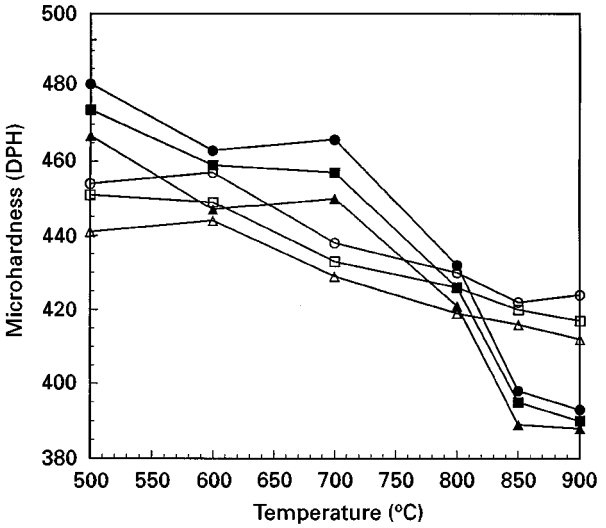

Figure 15 Microhardness of the matrix of the Ti–8.5Al–1B–1Si as a function of heat-treatment temperature for samples heat treated in (■, ●, ▲) air and (□, ○, △) argon for 5760 min: (■, □) mean, (●, ○) maximum, (▲, △) minimum.

followed by a gradual decrease to ≈ 420 DPH after 5760 min.

When considering the effect of time and temperature on the microhardness of the matrix there are three issues to be considered:

1. the increase in matrix microhardness due to solid-solution strengthening effect of oxygen in the α matrix;
2. the formation and dissolution of the α_2 phase;
3. the coarsening of the $TiSi_2$ and TiB particles with the consequential decrease in the supersaturation of the α matrix.

The three issues will now be discussed with respect to the observed results.

3.3.1. Oxygen as a solid-solution strengthener

Oxygen is an α stabilizer and also aids in the precipitation of the α_2 phase. The Ti–O phase diagram [29] indicates that the maximum solubility of oxygen in the lattice of pure titanium is ≈ 14 wt % and remains unchanged in the 550–1700 °C range. Oxygen, by virtue of its small size, can provide interstitial solid-solution strengthening. This effect is apparent even at short heat-treatment times for samples treated in air. The effect is less pronounced and slower in argon-treated samples as the oxygen content in the argon is less than 0.1% by volume. The peak hardness in the argon heat-treated samples is always lower than the air heat-treated samples.

3.3.2. The formation and dissolution of the α_2 phase

The as-received sample was extruded at 955 °C, which is in the single-phase α region, and cooled rapidly, hence the α_2 phase probably was not precipitated out. The Ti–Al phase diagram indicates that the ordered α_2 phase forms at $T < 750$ °C in this alloy. Heat treatments at $T < 750$ °C indicate that high strengths are developed and the α_2 phase is formed. At $T > 750$ °C it can be seen that the α_2 phase does not contribute to strengthening and there is a rapid drop in microhardness for the 2880 and 5760 min heat treatments. In the argon heat-treated samples, the drop in hardness is not as precipitous at $T > 750$ °C compared to the air heat-treated samples, because the kinetics of oxygen solubility is much slower due to the low oxygen content in the argon gas. It should, however, be noted that the hardness of the argon heat-treated samples never reaches that of the peak hardness of the air heat-treated sample.

3.3.3. The coarsening of the $TiSi_2$ and TiB particles

The coarsening of the $TiSi_2$ leads to a decrease in supersaturation of silicon in the α matrix. Silicon behaves as a substitutional solid-solution strengthener and as the $TiSi_2$ particles coarsen, the contribution of silicon as a solid-solution strengthener decreases. This coarsening behaviour of the $TiSi_2$ particles shows a similar trend in both air and argon and hence the contribution is similar in both cases. Boron is also a solid-solution strengthener and as the TiB particles coarsen, the contribution of boron as a solute to the matrix hardness, decreases.

3.4. Oxidation of titanium alloys

One of the principle limitations of the use of titanium alloys and titanium intermetallics is their poor oxidation resistance and embrittlement at elevated temperatures. The principal problems are (a) loss of structural material by oxide scale growth, and (b) embrittlement of the alloy surface layer by dissolved oxygen.

The oxidation of pure titanium has been extensively studied, and a good review can be found elsewhere [32]. In the 750–950 °C temperature range, the oxidation of pure titanium obeys a parabolic rate law followed by a linear region. During the parabolic period the reaction is controlled by diffusion of the reacting species through a compact TiO_2 layer which adheres with the base metal and generally conforms to Wagner's theory of oxidation. It has been found that once the oxide layer is about 15–20 μm thick, continuous cracks appear between the oxide layer and the metal base. Further oxidation leads to the formation of stratified scales. The oxidation following the cracking and stratification of oxide scales follows a pseudo linear law [33]. This description of oxidation largely applies to titanium alloys as well. However, the growth rate of the oxide and the oxygen diffusion coefficient in the substrate and the oxide may be appreciably altered depending on the specific alloy's content [32].

3.4.1. Kinetics of oxidation

The rate of oxidation is measured by weight gain which may be caused by oxide-scale growth as well as oxygen dissolution in the alloy. Hence two

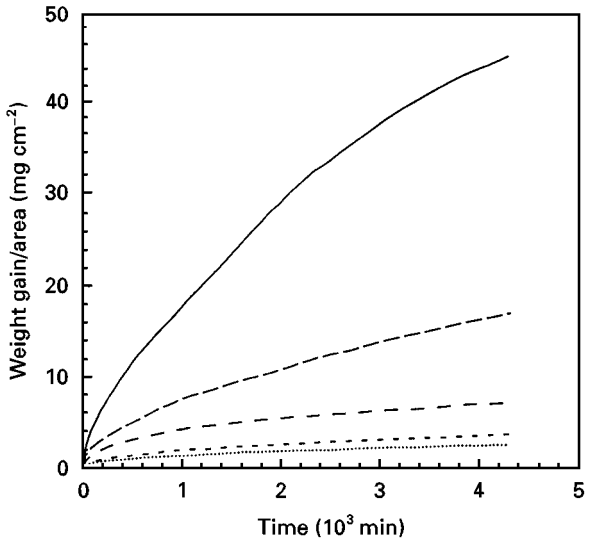

Figure 16 Weight gain per unit area as a function of time due to oxidation in flowing air at 50 $cm^3\,min^{-1}$ in the temperature range 750–950 °C: (···) 750 °C, (- - -) 800 °C, (– – –) (850 °C), (— — —) 900 °C, (——) 950 °C.

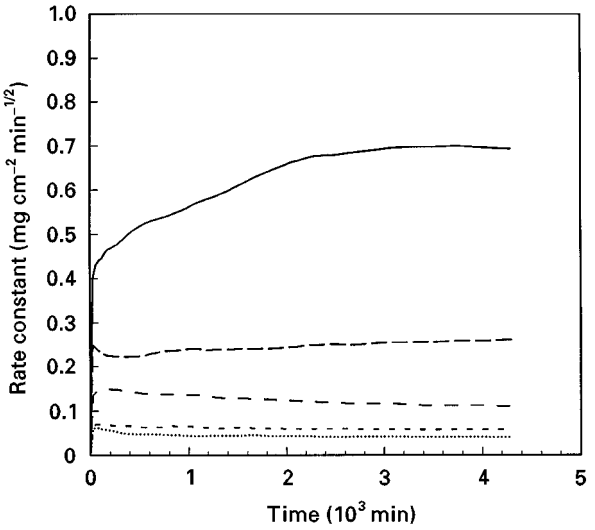

Figure 17 Parabolic oxidation rate constant as a function of time during oxidation in flowing air at 50 $cm^3\,min^{-1}$ in the temperature range 750–950 °C: (···) 750 °C, (- - -) 800 °C, (– – –) (850 °C), (— — —) 900 °C, (——) 950 °C.

weight-gain laws have to be employed, each with its specific rate constant and rate exponent. However, it is difficult to separate the contribution from each of the two processes. Hence, the weight gain in titanium-based alloys is usually described by a rate equation of the form [34–36]

$$W = k_p t^n \tag{2}$$

where W is the weight gain per unit area, k_p the oxidation rate constant, n the rate exponent, and t the time. In certain cases the value of n is a constant at different temperatures of testing, and under those conditions, k_p follows an Arrhenius relation of the form

$$k_p = k_0 \exp\left(\frac{-Q_{eff}}{RT}\right) \tag{3}$$

where Q_{eff} = effective activation energy for oxidation and k = constant for a given material.

3.4.1.1. Oxidation in flowing air. Fig. 16 shows a plot of the weight gain per unit initial surface area versus the annealing time for oxidation in temperature range 750–950 °C in an environment of 50 $cm^3\,min^{-1}$ flowing air. At temperatures below 750 °C, the amount of weight gain was below the resolution limit of the balance in use. However, the surface of the specimen did show discolouration, indicating that a limited amount of oxidation did occur. The weight gain data in Fig. 16 appear to fit a parabolic behaviour. Subtle variations of the oxidation behaviour are better revealed by plotting the oxidation rate constant as a function of time. Fig. 17 is a plot of k_p as a function of time at various temperatures. It can be clearly seen that in the temperature range 750–900 °C a clear parabolic oxidation behaviour is observed. This indicates the formation of protective oxide scale and oxidation kinetics are controlled by the diffusion of the active species through the oxide scale. However, at 950 °C it is clear that a pseudo parabolic behaviour is seen with the oxidation rate constant which increases with time. This indicates that there is a breakdown of the protective oxide scale at 950 °C. Beyond this temperature there is a rapid increase in the oxidation kinetics and no attempt was made to quantify this behaviour.

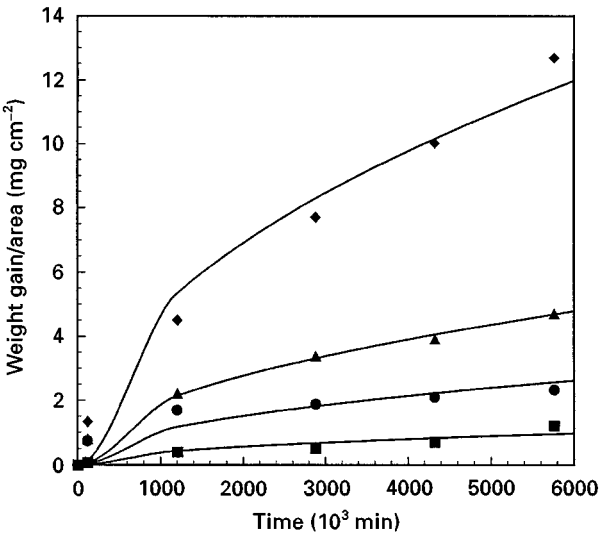

Figure 18 Weight gain per unit area as a function of time due to oxidation in static air in the temperature range 750–900 °C: (■) 750 °C, (●) 800 °C, (▲) 850 °C, (◆) 900 °C.

3.4.1.2. Oxidation in static air. Oxidation tests were conducted in a sealed quartz tube where the total content of air was 200 cm^3. Fig. 18 is a plot of weight gain as a function of time at various oxidation temperatures. The total weight gain at comparable temperatures is significantly lower in static air in comparison to an environment of flowing air. The difference in kinetics arises from a difference in the arrival rate of oxygen atoms at the surface of the sample. When flowing air is used there is a constant supply of oxygen atoms at the oxidation front, whereas in a sealed tube,

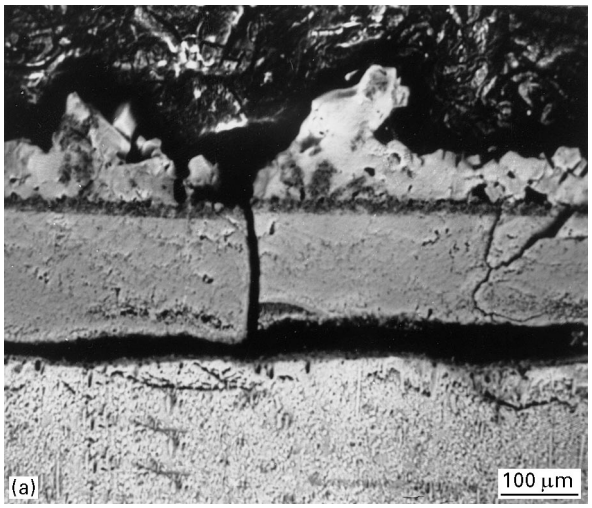

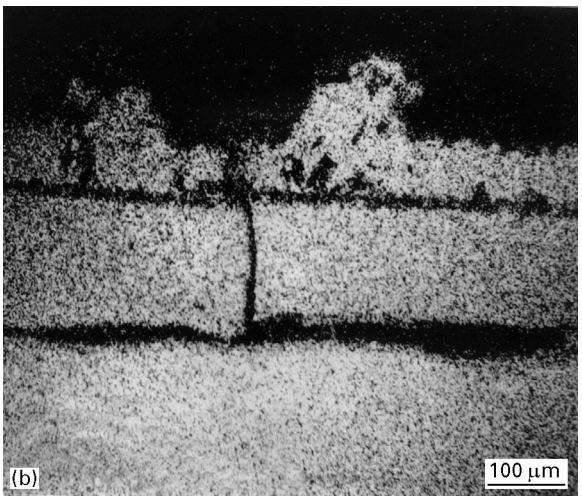

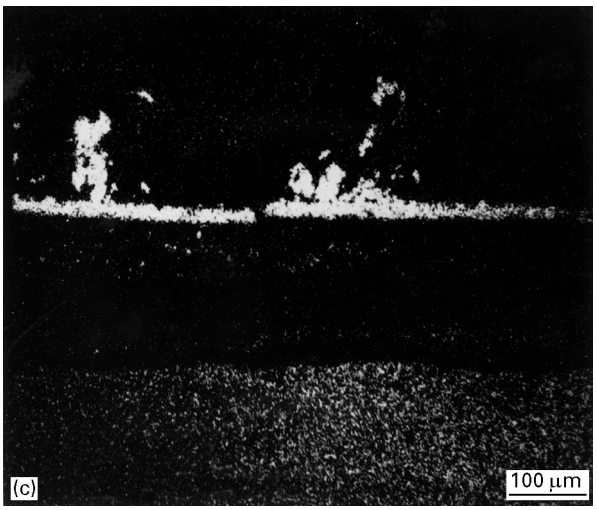

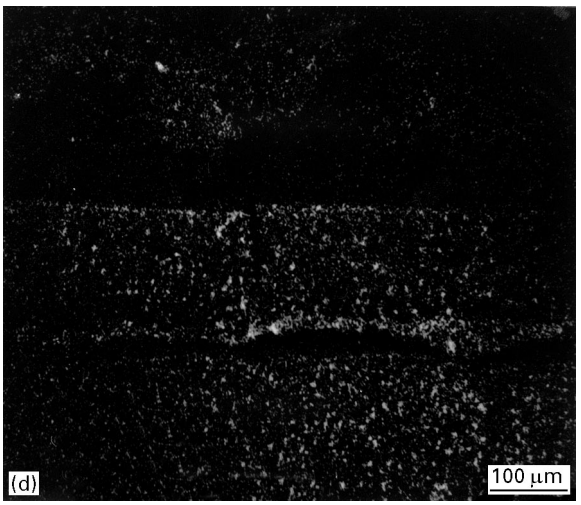

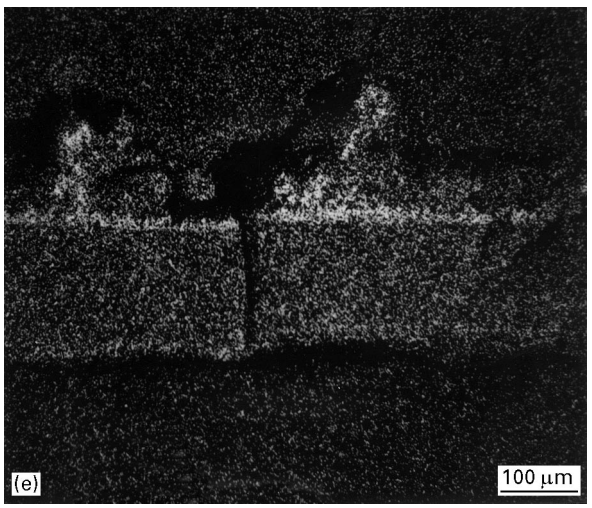

Figure 19 (a) Secondary electron image of the oxide scale and base material of the Ti–8.5Al–1B–1Si alloy exposed for 4320 min in an environment of flowing air at 950 °C. (b) Titanium X-ray dot map, (c) aluminium X-ray dot map (d) silicon X-ray dot map, (e) oxygen X-ray dot map.

there is a continuous drop in oxygen partial pressure as it is consumed, and the arrival rate of oxygen atoms at the oxidation surface is controlled by the convective currents in the tube.

3.4.2. Oxide-scale morphology

In both static and flowing air tests the specimen's surface exhibited various different colours depending on the oxidation temperature and times. Oxidation at temperatures below 700 °C for 120 min resulted in specimen surface discolouration which is blue in colour. Above 700 °C (including oxidation at 700 °C for more than 48 h) the surface was covered by a blue and grey scale. This blue/grey colouration became lighter as the temperature and/or oxidation time was increased. At temperatures above 1075 °C the specimen was covered by a thick yellow layer. Oxide scales obtained after annealing in the temperatures range 800–900 °C are very brittle and spall very easily.

Samples exposed for 96 h at 950 °C in flowing air have a well-defined oxide scale; cross-sections were made and back-scattered micrographs showing the base metal and the oxide scale, together with titanium, aluminum, silicon and oxygen X-ray dot maps are shown in Fig. 19a–e, respectively. Several distinctive regions are visible. These include region 1 in contact with air, which is pure TiO_2 and is between 20 and 80 μm thick. This is followed by a thin region, 2, of pure Al_2O_3 which is approximately 10–15 μm thick. This is followed by region 3, which is primarily TiO_2 with small particles of SiO_2 scattered in it. Region 4 is

the base material which has TiB rods and spherical $TiSi_2$ particles. It is important to note that the TiB rods are completely dissolved in the oxide without any trace. As the atomic number of boron is smaller than the resolution limit of the microprobe, it was not analysed. It is important to note that regions 1 and 2 also do not contain any silicon. This indicates clearly that the formation of regions 1 and 2 involves the outward growth of the oxides of titanium and aluminium, while region 3 is due to the growth of the oxide into the base material.

3.4.3. Activation energy for oxidation

Fig. 20 is a plot of K_p versus $1/T$; the slope of the plot yields the activation energy of oxidation. Table II also lists the activation energies for oxidation in the current tests as well as for various other systems. When oxidized in an environment of flowing air, the activation energy was found to be 200 kJ mol^{-1}.

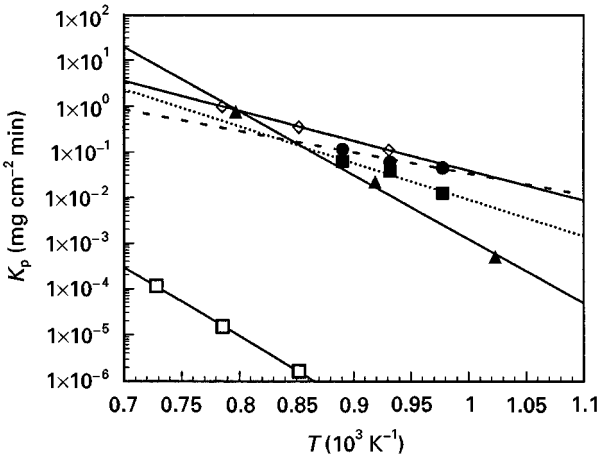

Figure 20 K_p versus $1/T$ for the Ti–8.5Al–1B–1Si. Superimposed are data for several other systems: (■) Ti–8.5Al–1B–1Si (static air), (●) Ti–8.5Al–1B–1Si (50 cm^3 min^{-1} air), (▲) Ti–48Al, (◇) TiO_2, (□) Al_2O_3.

TABLE II Activation energy for oxidation and diffusion in various titanium alloys

Alloy stoichiometry (wt %)	Activation energy (kJ mol^{-1})
Pure Ti [37]	239
Ti–1.5 wt % Al	183
Ti–9.7 wt % Al	209
Ti–15.81 wt % Al	269
Ti–16.52 wt % Al	255
Ti–22.5 wt % Al	299
Ti–35Al (400 p.p.m. oxygen) [38]	324
Ti–8.5Al–1B–1Si (in closed furnace) (present work)	303
Ti–8.5Al–1B–1Si (50 cm^3 min^{-1} air flow) (present work)	200
O diffusion in TiO_2 [39]	234
Ti diffusion in TiO_2 [41]	257
O diffusion in Al_2O_3 above 1400 °C [42]	460
O diffusion in Al_2O_3 above 1400 °C [43]	587
O fast diffusion paths in Al_2O_3 [44]	241
Al diffusion in polycrystalline Al_2O_3 [42]	477

When oxidized in a static air environment, the activation energy is 303 kJ mol^{-1}. The activation energy in flowing air is equal to the activation energy in a Ti–9.7Al alloy shown in Table II. This low value of activation energy is due to the formation of cracks in the oxide which lead to short cuts in the oxidation pathways. This behaviour is seen in Fig. 19 where a crack is evident in the TiO_2 oxide scale. When oxidized in an environment of static air, the oxidation is controlled by the arrival of oxygen atoms to the oxidation front and the rate of growth of the oxide is slower than in flowing air. In addition, the formation of a compact oxide scale of TiO_2 yields a higher activation energy.

4. Conclusions

The microstructural stability of Ti–8.5Al–1B–1Si (wt %) in the temperature range 500–900 °C was studied. The variation of microhardness of the matrix was studied as a function of time and temperature in air and argon atmospheres. The following results can be inferred from the experiments.

1. The coarsening behaviour of the $TiSi_2$ particles is primarily by grain-boundary diffusion at 750 °C and follows a rate equation of the form $\bar{d}^4 - \bar{d}_0^4 = kt$ with $k = 2.38 \times 10^{-30}$ m^4 s^{-1} in air and in argon at 750 °C.
2. Oxygen behaves as a solid-solution strengthener and its effect is more pronounced in the air heat-treated samples compared to the argon heat-treated samples.
3. When heat treated in air, there is a sharp drop in matrix hardness at $T > 750$ °C for all times. This could be attributed to two reasons; (a) the α_2 phase present in the matrix dissolves on moving into the single-phase α-phase field, and (b) the coarsening of the silicides and borides depletes the matrix of silicon and boron decreasing the solid-solution strengthening.
4. This alloy has an activation energy for oxidation of 303 kJ mol^{-1} when oxidized in a closed chamber and an activation energy of 200 kJ mol^{-1} when oxidized in flowing air with a flow rate of 50 cm^3 min^{-1}.

Acknowledgements

This work was supported in part by a research initiation grant from the National Science Foundation (MSS-9108891), Mr William Spitzig, Contract Monitor. Experimental assistance provided by Mr Keith Logan, Mr Salvador Anguiano and Mr Sriram Rangarajan is gratefully acknowledged.

References

1. D. EYLON, P. FUJISHIRO, P. POSTANTS and F. FROES, *J. Metals*, **36**(11) (1984) 55.
2. S. WHANG, *J. Mater. Sci.* **21** (1986) 2224.
3. S. M. L. SASTRY, T. PENG, P. MESCHTER and J. O'NEAL, *J. Metals* **35**(9) (1983) 21.
4. S. M. L. SASTRY, P. MESCHTER and J. O'NEAL, *Metall. Trans.* **15** (1984) 1451.

5. S. M. L. SASTRY, T. PENG, and J. O'NEAL, in "Titanium Science and Technology", Proceedings of the 5th International Conference on Titanium, edited by U. Zwicker, G. Lutgering and W. Bunk, Vol. I (D. G. fur Metallkunde, 1985) p. 397.
6. S. WHANG, *J. Metals* **36**(4) (1984) 34.
7. H. LIPSITT, in "Proceedings of the Research Society Symposium", Vol. 39 (Materials Research Society, 1985) p. 351
8. D. KONITZER, B. MUDDLE, H. FRASER and R. KIRCHHEIM in "Titanium Science and Technology", Proceedings of the 5th International Conference on Titanium, edited by U. Zwicker, G. Lutgering and W. Bunk, Vol. 1 (D.G. fur Metallkunde, 1985) p. 405.
9. Y. LU and B. GIESSEN, in "Rapidly Solidified Alloys and Their Mechanical and Magnetic Properties", Vol. 58, edited by B. Giessen, D. Polk and A. Taulb (Materials Research Society, Pittsburgh, PA 1986) p. 377.
10. J. SUTLIFF and R. G. ROWE, *ibid*., p. 371.
11. R. G. ROWE, J. SUTLIFF and E. KOCH, in "Titanium Rapid Solidification Technology", edited by F. Froes and D. Eylon, (The Metallurgical Society, 1986) p. 240.
12. C. SHAMBLEM and T. REDDEN, "Science, Technology and Application of Titanium" (1969).
13. S. RANGARAJAN, P. B. ASWATH and W. O. SOBOYEJO, *Scripta Metall. Mater*., in press.
14. S. RANGARAJAN, P. B. ASWATH and W. O. SOBOYEJO, *J. Mater. Res*., submitted.
15. W. O. SOBOYEJO, R. J. LEDERICH and S. M. L. SASTRY, *Acta Metall.* **42** (1994) 2579.
16. T. PENG, B. LONDON and S. M. L. SASTRY, in "Advances in Powder Metallurgy", Proceedings of the Conference on Powder Metallurgy, Vol. 3, edited by T. Gasbarre and W. Jandeska (American Powder Metallurgy Institute, Princeton, 1990) p. 387.
17. C. SURYANARAYANA and S. FROES, *J. Metals* **42**(3) (1990) 26.
18. S. SAVAGE and F. FROES, *ibid*. **36**(4) (1984) 20.
19. A. JACKSON, T. BRODERICK and F. FROES, in "Titanium Science and Technology", Proceedings of the 5th International Conference on Titanium, Vol. 1, edited by U. Zwicker, G. Lutgering and W. Bunk (D.G. fur Metallkunde, 1985) p. 381.
20. S. M. L. SASTRY, D. BOWDEN and R. J. LEDERICH, *ibid*., p. 435.
21. M. IMAM, B. B. RATH and D. GILLESPIE, *ibid*., p. 1511.
22. J. MURRAY, in "Binary Phase Diagrams", edited by T. Massalski (American Society of Metals, Metals Park, OH, 1987) p. 175.
23. G. T. GRAY III, G. LUETJERING and J. C. WILLIAMS, *Metall. Trans.* **21A** (1990) p. 95.
24. J. MURRAY, P. LIAO and K. SPEAR, in "Binary Phase Diagrams", edited by T. Massalski (American Society of Metals, Metals Park, OH, 1987) p. 392.
25. J. E. O'NEAL, S. M. L. SASTRY and T. PENG, in "Microstructural Science", Vol. 15, edited by M. Blum, P. French and R. Middleton (The International Metallographic Society, Columbus, OH, 1987) p. 275.
26. J. MURRAY, in "Binary Phase Diagrams", edited by T. Massalski (American Society of Metals, Metals Park, OH, 1987) p. 2056.
27. M. MENDIRATTA, S. M. L. SASTRY and J. SMITH, *J. Mater. Sci.* **11** (1976) 1835.
28. G. SCARR, J. WILLIAMS, S. ANKEM and H. BOMBERGER, in "Titanium Science and Technology", Proceedings of the 5th International Conference on Titanium, edited by U. Zwicker, G. Lutgering and W. Bunk, Vol. 3 (D.G. fur Metallkunde 1985) p. 1475.
29. J. MURRAY, in "Binary Phase Diagrams", edited by T. Massalski (American Society of Metals, Metals Park, OH, 1987) p. 1793.
30. S. BHATTACHARYA and K. RUSSEL, *Metall. Trans. A.* **3** (1972) 1972.
31. E. COLLINS, in "Alloying", edited by J. Walter, M. Jackson and C. Sims (American Society of Metals, Metals Park, OH, 1988) p. 257.
32. P. KOFSTADT, "High Temperature Oxidation of Metals" (Wiley, New York, 1966).
33. M. PONS, B. B. RATH and A. GILLESPIE, *J. Less-Common Metals* **109** (1985) 45.
34. G. WELSCH and A. KAHVECI, in "Oxidation of High Temperature Intermetallics", edited by T. Grobstein and J. Doychak (The Minerals, Metals and Materials Society, Pittsburgh, PA, 1989) p. 207.
35. E. LEE and J. WALDMAN, *Scripta Metall.* **22** (1988) 1389.
36. R. SHENOY, J. UNNAM and R. CLARK, *Oxid. Metals* **26** (1986) 105.
37. A. M. CHAZE, C. CODDETT and G. BERANGER, *J. Less Common Metals* **83** (1982) 49.
38. S. A. KEKARE, D. K. SHELTON and P. B. ASWATH, "High Temperature Ordered Intermetallics V", edited by I. Baker, R. Darolia, J. D. Whittenberger and M. H. Yoo, Materials Research Society Proceedings, Vol. 288 (Materials Research Society, 1993) p. 10265.
39. J. UNNAM, R. N. SHENOY and R. K. CLARK, *Oxid. Metals* **26** (1986) 231.
40. N. S. CHOUDHARY, H. C. GRAHAM and J. W. HINZE, in "Proceedings of the Symposium on Properties of High Temperature Alloys", edited by Z. A. Foroulis and F. S. Petit, Electrochemical Society Proceedings, **77-1** (The Electrochemical Society, 1976) p. 668.
41. D. L. VENKATU and L. E. POTEAT, *Mater. Sci. Eng.* **5** (1969/1970) 258.
42. Y. OISHI and W. D. KINGERY, *J. Chem. Phys.* **3** (1960) 905.
43. K. P. D. LANGERLOF, T. E. MITCHELL and A. H. HEUR, in "Solute-Defect Interaction", edited by S. Saimoto, G. R. Purdy and G. V. Kidson (Pergamon Press, 1986) p. 152.
44. "High Temperature Oxidation-Resistant Coating", Committee on Coatings (National Materials Advisory Board, National Academy of Sciences, 1970) p. 29.

Received 24 June
and accepted 23 October 1996